Archives of Civil and Mechanical Engineering (2024) 24:114
https://doi.org/10.1007/s43452-024-00929-2

ORIGINAL ARTICLE

A better understanding of tunnel deformable supports: from analytical model to engineering application

Kui Wu[1] · Yuzhu Wang[1] · Xiaomeng Zheng[1] · Nannan Zhao[1]

Received: 15 November 2023 / Revised: 26 February 2024 / Accepted: 19 March 2024 / Published online: 10 April 2024

Abstract

The severe failure of strong supports occurred in the Xinhua tunnel that was a deep-buried tunnel excavated in squeezing ground. In order to address such problem, this study explores the possibility of applying deformable supports in this tunnel. The mechanical response of a circular "rockbolt and yielding lining" supported tunnel is studied from the perspective of the convergence-confinement method. The equations for calculating the elastic modulus, cohesion, and internal friction angle of bolted rock are provided firstly; the mechanical model of the bolted tunnel is established then, where the surrounding rock can be classified into the plastic bolted, elastic bolted, and elastic unbolted regions. The equations for constructing the ground reaction curve are provided considering rockbolt reinforcement and rock shear dilatancy. The reduced case that the surrounding rock does not generate the plastic region is discussed as well, if the support pressure is higher than the critical value. The required minimum support pressure is further determined following the assumptions of maximizing the utilization of rockbolt bearing capacity and generating no loosening rock pressure. The exact equations for determining the lining thickness and length of highly deformable elements are provided with the intention to ensure lining safety and accept rock displacement. Based on the consideration of shotcrete hardening property, the equation to calculate the yielding stress of highly deformable elements is provided. The equations for GRC in this study can be reduced to those without considering rockbolt reinforcement or rock shear dilatancy. The design model of yielding lining is well applied in the Xinhua tunnel. The analysis results show that the rock displaces for 382.6 mm and the lining generates a plastic displacement of 281.8 mm in the Xinhua tunnel using the strong supports, which have a good agreement with the field monitoring data. The required lining thickness is equal to 28 cm and the installation number and length of highly deformable elements are 9 and 41.3 cm, respectively, when the yielding lining is employed in the Xinhua tunnel. Finally, a parametric investigation is carried out, including the cohesion and internal friction angle of rock, rockbolt length, and initial ground stress. Some recommendations for the tunnel design are proposed.

Keywords Tunnel · Large deformation · Rockbolt · Deformable supports · Convergence-confinement method

1 Introduction

The yielding lining is considered as one type of the most potential support structures that are able to address the problem of rock large deformation without being damaged [1]. Several highly deformable elements are implemented in the lining around its circumference, which leads to the so-called yielding lining [2]. These highly deformable elements have great deformability and can exhibit considerable shortening at a low stress (compared with shotcrete compressive strength) [3]. Hence, the yielding lining utilizes the compression deformation of these elements to allow the rock displacement under a certain support pressure (associated with the yielding stress of elements) [4]. Once the ultimate strain of elements is completed, it (yielding lining) eventually becomes a strong structure that strictly limits rock displacement [5].

Recently, more research attention has moved from conventional strong supports to yielding lining [6]. Even, Cantieni and Anagnostou [7] considered that the only feasible solution to deep tunneling in severe squeezing ground is that the support structure has the capacity of displacing for a certain amount. The idea behind it is that

✉ Nannan Zhao
zhaonannan@xauat.edu.cn

[1] School of Science, Xi'an University of Architecture and Technology, Xi'an 710055, China

the rock pressure can be reduced to a controlled level by allowing rock displacement [8]. Unfortunately, so far there is still no unified and acceptable specification to guide the design of yielding lining, which greatly challenges its wide application in large deformation tunnels [9].

Of course, it also should highlight the reinforcement of surrounding rock in large deformation tunnels, although the yielding lining allows rock displacement. Rock mechanical performance can be improved to a certain extent after being reinforced, causing the increase in its bearing capacity and decrease in risk of rock from loosening to sudden collapse during deformation [10]. The utilization of rockbolt is the most common rock reinforcement method in tunnels [11]. The rockbolt reinforcement mechanism was investigated by many researchers, such as Chen et al. [12], Chen and Li [13], Lu et al. [14], and Li [15]. In these references, they established various theoretical models to describe the interaction between surrounding rock and rockbolts. However, these models were analytically complex and it is not easy and convenient to apply them to predict the mechanical behavior of bolted tunnels in the theoretical design stage.

The convergence-confinement method (CCM) for tunnel is a standard approach for preliminary analysis of anticipated tunnel displacement and support design [16]. The ground response to the advancing tunnel face and the interaction with installed supports are considered in the convergence-confinement method [17]. The convergence-confinement method has been widely applied in the design of strong supports [18]. Simultaneously, this method has been continuously improved by considering various influencing factors, such as rock behavior [19], time-dependent material behavior of shotcrete [20], cross-section shape [21], new type of strong supports [22], and installation delay of supports [23]. However, few work has been reported on the design of yielding lining by using the convergence-confinement method.

This study investigates the design of rockbolt-yielding lining supported tunnel using the convergence-confinement method. After the "Introduction," a brief history of yielding lining was available in Sect. 2. Section 3 provided the exact equations for ground reaction curve considering rockbolt reinforcement. In Sect. 4, the minimum support pressure was determined from the prospective of loosening pressure and rock plastic radius. The lining thickness and the length and yielding stress of highly deformable elements were determined using the convergence-confinement method in Sect. 5. An application of design method of yielding lining is applied in the Xinhua tunnel in Sect. 6. Section 7 carries out a parametric investigation on rock cohesion and internal friction angle, rockbolt length, and initial ground stress. Findings and recommendations are highlighted in the final section.

2 A brief history of yielding lining

The concept of rock displacement release was initially realized by leaving several longitudinal gaps in shotcrete lining [24]. However, the lining resistance would be decreased to a very low level in this way, because the tangential forces in the lining could not be transferred over these gaps [25]. The first practice to fill these open gaps with groups of axially loaded steel pipes was achieved in the Galgenberg tunnel (Austria) in 1994 [26]. This attempt was the earliest report on the so-called yielding lining.

In fact, the resistance of those groups of axially loaded steel pipes used in the Galgenberg tunnel exhibited pronounced oscillations during their shortenings [27]. Thereafter, a series of highly deformable elements were further developed in order to achieve stable resistance [28]. According to their production materials, these highly deformable elements could be roughly classified into two groups: porous fillings and steel elements [29]. The Hid-Con element was the most used highly deformable element in porous fillings type. Its compressibility could amount to approximately 50% at a stable yielding stress of 8.5 MPa [30]. The common steel elements had the Lining Stress Controller (LSC) [29], the Wabe element [4], and the Support Resistant Limiting Samper (SRLD) [31].

The yielding lining characterized more complex deformation behavior due to the incorporation of highly deformable elements in the lining. At present, the researches on yielding lining majorly adopted numerical and analytical approaches [32]. Numerical method has more advantages in simulating the mechanical response of yielding lining under complex working conditions [33]. Liu et al. [34], Ramoni and Anagnostou [35], Tian et al. [36], Yang et al. [37], and Hammer et al. [38] used numerical approach modeled the interaction between surrounding rock and yielding lining and highlighted the importance of yielding length and stress of highly deformable elements on lining damage. In terms of analytical method, it is easy to understand the mechanics of deformation behavior of yielding lining and obtain a better understanding of the influence of involved parameters on its final performance [39]. According to the compressive characteristics of highly deformable elements, Wu et al. [40] simplified the whole deformation process of yielding lining into three stages (elastic–yielding–elastic) and provided the corresponding stiffness calculation method. Furthermore, they provided an analytical solution considering the influence of shotcrete hardening property on yielding lining behavior [41]. Attempts on establishment of analytical models of yielding lining were also conducted by Cantieni and Anagnostou [7], Lei and Zhao [42] and Mezger et al. [43], Tian et al. [44], Radoncic et al. [45], and Sakai and Schubert

[46]. Unfortunately, a widely recognized design method of yielding lining has been still unavailable.

As shown in Fig. 1, good applications of yielding lining had been obtained in more tunnels throughout the world, for instance the Koralm tunnel (Austria) [47], the Tauern tunnel (Austria) [48], the Lötschberg Base tunnel (Switzerland) [49], and the Yangshan tunnel (China) [31]. It should be admitted that yielding lining was not the preferred solution to the problem of rock severe squeezing occurred in these tunnels. However, the aforementioned tunnels eventually replaced original strong supports with yielding lining, because they were unable to provide sufficient resistance to limit rock displacement and generated irreparable failure. Most notably, it was full of difficulties to apply the yielding lining in the Saint Martin La Porte access tunnel. The installation number and positions of highly deformable elements incorporated into lining were changed several times, because the lining was still subjected to severe damage following improper element arrangements [49]. In addition, the design of yielding lining in the Bolu tunnel (Turkey) was unreasonable, which directly led to the utilization of a super strong lining (the total thickness of shotcrete lining and Bernold lining reaching 1.0 m, not including the secondary lining) in this tunnel [50]. These examples clearly illustrate that the current design method of yielding lining is still full of significant challenges.

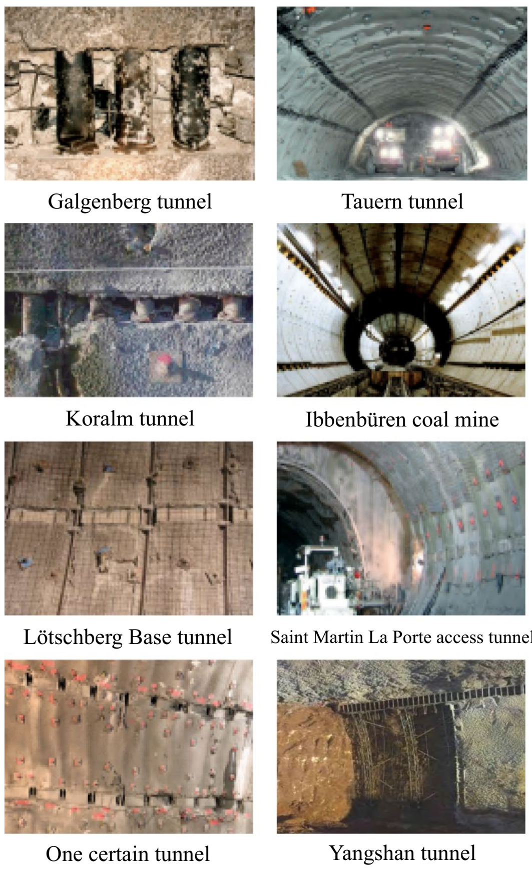

Fig. 1 Applications of yielding lining in tunnel projects

3 Ground reaction curve (GRC) considering rockbolt reinforcement

3.1 Mechanical parameters of bolted rock

The cohesion and internal friction angle of rock can be improved after using rockbolt reinforcement from the prospective of mechanics [51]. Rockbolts and bolted rock form a new composite that exhibits a stronger anti-deforming capacity. Figure 2 shows the arrangement of rockbolts in a circular tunnel. Based on the theory of equivalent

Fig. 2 Arrangement of rockbolts in tunnel

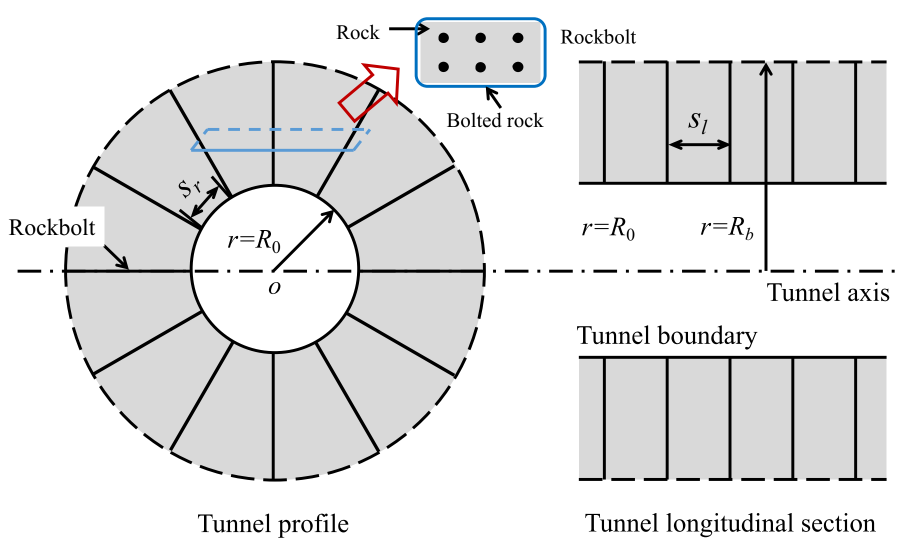

elastic modulus of composites, it is easy to provide the elastic modulus of bolted rock as follows:

$$E^*A^* = EA + E_b A_b, \tag{1}$$

where E^*, E, and E_b denote the elastic moduli of bolted rock, rock, and rockbolt, respectively. A^*, A, and A_b represent the areas of bolted rock, rock, and rockbolt, respectively.

Considering the arrangement parameters of rockbolts in the tunnel, the elastic modulus of bolted rock can then be obtained as shown in Eq. (2):

$$E^* = \frac{E_b \pi r_b^2 + E\left(s_l s_r - \pi r_b^2\right)}{s_l s_r}, \tag{2}$$

where s_r and s_l are the tangential and longitudinal spacings of rockbolt, respectively. R_b represents the radius of rockbolt. After rockbolt installation, the Poisson's ratio of bolted rock is still considered to be equal to that of rock (ν).

For the rock material subjected to the Mohr–Coulomb strength criteria, it has

$$\sigma_\theta = P(\varphi)\sigma_r + Q(c, \varphi), \tag{3}$$

where σ_r and σ_θ represent the radial and tangential stresses, respectively. c and φ are the cohesion and internal friction angle of rock, respectively. In Eq. (3), $P(\varphi) = (1 + \sin\varphi)/(1 - \sin\varphi)$ and $Q(c, \varphi) = 2c\cos\varphi/(1 - \sin\varphi)$.

Indraratna and Kaiser [52] had investigated the mechanical properties of bolted rock and provided the formulas to calculate the parameters of $P(\varphi^*)$ and $Q(c^*, \varphi^*)$ in the Mohr–Coulomb strength criteria of bolted rock, as shown in Eq. (4):

$$\begin{cases} P(\varphi^*) = (1+\eta)P(\varphi) \\ Q(c^*, \varphi^*) = (1+\eta)Q(c, \varphi) \end{cases}, \tag{4}$$

where η is defined as the rockbolt density factor, which has the following expression:

$$\eta = \frac{2\pi r_b \tan\varphi/2}{s_r s_l}. \tag{5}$$

Furthermore, the internal friction angle and cohesion of bolted rock (φ^*, c^*) can be obtained as follows:

$$\varphi^* = \arcsin\left[\frac{(1+\sin\varphi)\eta + 2\sin\varphi}{(1+\sin\varphi)\eta + 2}\right], \tag{6}$$

$$c^* = \frac{c(1+\eta)(1-\sin\varphi^*)\cos\varphi}{(1-\sin\varphi)\cos\varphi^*}. \tag{7}$$

3.2 Derivation of GRC considering rockbolt reinforcement

This section involves the derivation of the ground reaction curve (GRC) considering rockbolt reinforcement. Before the derivation, some considerations should be made. The instantaneous installation of rockbolts is completed after tunnel excavation. If it generates the plastic zone in the surrounding rock (it implies that the support pressure P_i is smaller than the critical pressure P_{cri}), the zone radius of rockbolt-reinforced surrounding rock (R_b) is considered to be larger than the plastic radius (R_p). The other case is that it does not generate the plastic zone in the surrounding rock and the plastic radius is equal to the tunnel radius R_0, as the support pressure is larger than or equal to this critical pressure. Figure 3 illustrates the mechanical model of a circular

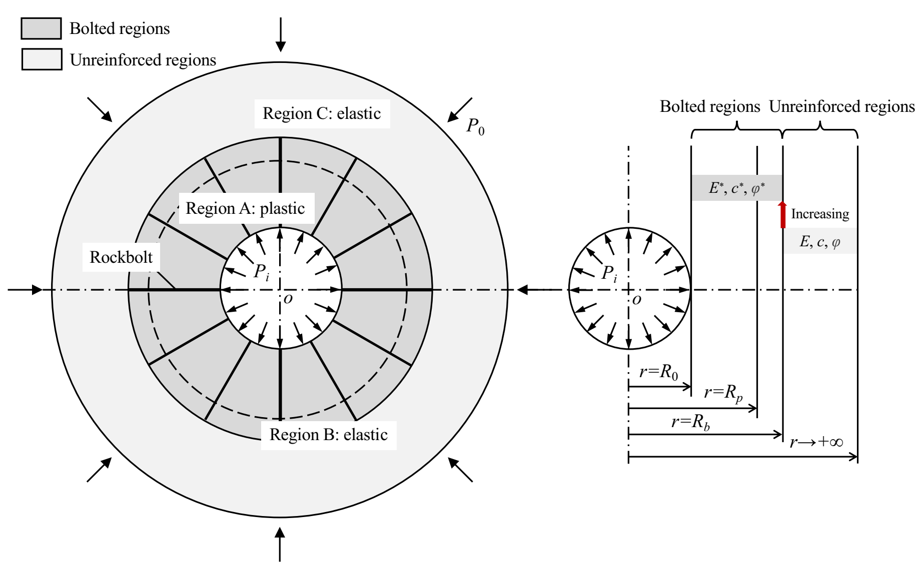

Fig. 3 Mechanical model of a circular rockbolt-reinforced tunnel

rockbolt-reinforced tunnel, in which a part of the surrounding rock is in the plastic state. In this model, the surrounding rock is divided into three zones. The bolted surrounding rock in region A is in the plastic state. The bolted surrounding rock in region B and the unbolted in region C are both in the elastic state.

The theory of tunnel mechanics had provided formulas for the radial stress in the interface between the elastic and plastic zones ($r=R_p$) and plastic radius in a circular tunnel, which surrounding rock is homogeneous and subjected to the Mohr–Coulomb strength criteria [53]. If submitting the parameters of bolted surrounding rock into these formulas, it can obtain the formulas for the radial stress in the interface between the elastic and plastic zones and plastic radius in the bolted-reinforced tunnel, as shown in Eqs. (8) and (9). The radial stress in Eq. (8) is equal to the aforementioned critical support pressure. The plastic zone will not occur, if the support pressure is greater than or equal to this threshold value.

$$\sigma_{rp} = \frac{2P_0 - Q(c^*, \varphi^*)}{1 + P(\varphi^*)} = P_0(1 - \sin\varphi^*) - c^* \cos\varphi^*, \tag{8}$$

$$R_\mathrm{p} = R_0 \left[\frac{\left(P_0 + c^* \cot\varphi^*\right)(1 - \sin\varphi^*)}{P_i + c^* \cot\varphi^*} \right]^{\frac{1-\sin\varphi^*}{2\sin\varphi^*}}, \tag{9}$$

where P_0 denotes the initial ground stress.

In addition, for a circular tunnel within the homogeneous surrounding rock, the theory of tunnel mechanics had provided the elastic stress and displacement fields around the tunnel, as shown in Eqs. (10) and (11) [54]:

$$\begin{cases} \sigma_r^\mathrm{e} = P_0\left[1 - \left(\frac{R_\mathrm{p}}{r}\right)^2\right] + \sigma_{rp}\left(\frac{R_\mathrm{p}}{r}\right)^2 \\ \sigma_\theta^\mathrm{e} = P_0\left[1 + \left(\frac{R_\mathrm{p}}{r}\right)^2\right] - \sigma_{rp}\left(\frac{R_\mathrm{p}}{r}\right)^2 \end{cases}, \tag{10}$$

$$u_r^\mathrm{e} = \frac{1+\nu}{E}\left(P_0 - \sigma_{rp}\right)\frac{R_\mathrm{p}^2}{r}, \tag{11}$$

where σ_r^e and σ_θ^e denote the radial and tangential stresses in the elastic zone, respectively. u_r^e is the radial displacement in the elastic zone. r is the distance of the rock element from the tunnel center.

When the surrounding rock has an elastic modulus E, the radial displacement at $r=R_\mathrm{b}$ can be obtained using Eq. (11) as follows:

$$u_{rb}^\mathrm{e} = \frac{1+\nu}{E}\left(P_0 - \sigma_\mathrm{rp}\right)\frac{R_\mathrm{p}^2}{R_\mathrm{b}}. \tag{12}$$

If the elastic modulus of whole surrounding rock is equal to E^*, the radial displacement in the elastic zone and at $r=R_\mathrm{b}$ can be given by Eqs. (13) and (14), respectively:

$$u_r^\mathrm{e*} = \frac{1+\nu}{E^*}\left(P_0 - \sigma_{rp}\right)\frac{R_\mathrm{p}^2}{r}, \tag{13}$$

$$u_{rb}^\mathrm{e*} = \frac{1+\nu}{E^*}\left(P_0 - \sigma_{rp}\right)\frac{R_\mathrm{p}^2}{R_\mathrm{b}}. \tag{14}$$

Actually, for a rockbolt-reinforced tunnel, only the elastic modulus of bolted surrounding rock (from R_0 to R_b) is equal to E^*. Combining Eqs. (12)–(14), it can obtain the radial displacement in Region B in Fig. 3 as follows:

$$\begin{aligned} u_r &= u_r^\mathrm{e*} + \left(u_{rb}^\mathrm{e} - u_{rb}^\mathrm{e*}\right)\frac{r}{R_\mathrm{b}} \\ &= \frac{1+\nu}{E^*}\left(P_0 - \sigma_{rp}\right)\frac{R_\mathrm{p}^2}{r} \\ &+ \left[\frac{1+\nu}{E}\left(P_0 - \sigma_{rp}\right)\frac{R_\mathrm{p}^2}{R_\mathrm{b}^2} - \frac{1+\nu}{E^*}\left(P_0 - \sigma_{rp}\right)\frac{R_\mathrm{p}^2}{R_\mathrm{b}^2}\right] r. \end{aligned} \tag{15}$$

Subsequently, submitting $r=R_p$ into Eq. (15) provides the radial displacement in the elastic–plastic interface of the bolted surrounding rock, as presented in Eq. (16).

$$u_{rp}^\mathrm{e} = \left[\frac{1+\nu}{E^*}\frac{R_\mathrm{b}^2 - R_\mathrm{p}^2}{R_\mathrm{b}^2} + \frac{1+\nu}{E}\frac{R_\mathrm{p}^2}{R_\mathrm{b}^2}\right] R_\mathrm{p}\left(P_0 - \sigma_{rp}\right). \tag{16}$$

The plastic strain of the surrounding rock in the plastic zone (region A) satisfies Eq. (17), when considering the rock shear dilatancy.

$$\varepsilon_\mathrm{r}^\mathrm{p*} + \alpha\varepsilon_\theta^\mathrm{p*} = 0, \tag{17}$$

where ε_r^{p*} and ε_θ^{p*} represent the radial and tangential plastic strains of the bolted surrounding rock, respectively. α denotes the dilatancy coefficient.

Equation (17) can be rewritten as

$$\left(\varepsilon_r - \varepsilon_{rp}^\mathrm{e*}\right) + \alpha\left(\varepsilon_\theta - \varepsilon_{\theta\mathrm{p}}^\mathrm{e*}\right) = 0, \tag{18}$$

where $\varepsilon_{rp}^\mathrm{e*}$ and $\varepsilon_{\theta\mathrm{p}}^\mathrm{e*}$ denote the radial and tangential elastic strains of the bolted surrounding rock in the elastic–plastic interface ($r=R_\mathrm{p}$), respectively.

For the plane strain problem of a circular tunnel, the geometric equation can provide the relationship between the strain and displacement as follows [55]:

$$\begin{cases} \varepsilon_r = \dfrac{\mathrm{d}u_r}{\mathrm{d}r} \\ \varepsilon_\theta = \dfrac{u_r}{r} \end{cases}. \tag{19}$$

Using Eqs. (15) and (19) can determine the radial and tangential elastic strains of the bolted surrounding rock in the elastic–plastic interface ($r = R_\mathrm{p}$) as follows:

$$\begin{cases} \varepsilon_{r\mathrm{p}}^{\mathrm{e}*} = -\dfrac{1+v}{E^*}\left(P_0 - \sigma_{r\mathrm{p}}\right) + \left[\dfrac{1+v}{E}\left(P_0 - \sigma_{r\mathrm{p}}\right)\dfrac{R_\mathrm{p}^2}{R_\mathrm{b}^2} - \dfrac{1+v}{E^*}\left(P_0 - \sigma_{r\mathrm{p}}\right)\dfrac{R_\mathrm{p}^2}{R_\mathrm{b}^2}\right] \\ \varepsilon_{\theta\mathrm{p}}^{\mathrm{e}*} = \dfrac{1+v}{E^*}\left(P_0 - \sigma_{r\mathrm{p}}\right) + \left[\dfrac{1+v}{E}\left(P_0 - \sigma_{r\mathrm{p}}\right)\dfrac{R_\mathrm{p}^2}{R_\mathrm{b}^2} - \dfrac{1+v}{E^*}\left(P_0 - \sigma_{r\mathrm{p}}\right)\dfrac{R_\mathrm{p}^2}{R_\mathrm{b}^2}\right] \end{cases}. \tag{20}$$

Subsequently, submitting Eqs. (19) and (20) into (18) provides the governing equation of the radial displacement of surrounding rock in the plastic zone, as shown in Eq. (21).

$$\frac{\mathrm{d}u_r}{\mathrm{d}r} + \alpha\frac{u_r}{r} = \frac{(\alpha-1)(1+v)}{E^*}\left(P_0 - \sigma_{r\mathrm{p}}\right) + (\alpha+1)\left[\frac{1+v}{E}\left(P_0 - \sigma_{r\mathrm{p}}\right)\frac{R_\mathrm{p}^2}{R_\mathrm{b}^2} - \frac{1+v}{E^*}\left(P_0 - \sigma_{r\mathrm{p}}\right)\frac{R_\mathrm{p}^2}{R_\mathrm{b}^2}\right]. \tag{21}$$

The above equation deals with a first-order differential equation. Its boundary condition is presented in Eq. (16) and its exact solution can be calculated as

$$u_r = \frac{2(1+v)\left(P_0 - \sigma_{r\mathrm{p}}\right)R_\mathrm{p}^{\alpha+1}}{E^*(\alpha+1)r^\alpha} + \left[\frac{(\alpha-1)(1+v)}{E^*(\alpha+1)} + \frac{1+v}{E}\frac{R_\mathrm{p}^2}{R_\mathrm{b}^2} - \frac{1+v}{E^*}\frac{R_\mathrm{p}^2}{R_\mathrm{b}^2}\right]\left(P_0 - \sigma_{r\mathrm{p}}\right)r. \tag{22}$$

Submitting $r = R_0$ into Eq. (22) provides the radial displacement at the tunnel wall as follows:

$$u_{\max} = \frac{2(1+v)\left(P_0 - \sigma_{r\mathrm{p}}\right)R_\mathrm{p}^{\alpha+1}}{E^*(\alpha+1)R_0^\alpha} + \left[\frac{(\alpha-1)(1+v)}{E^*(\alpha+1)} + \frac{1+v}{E}\frac{R_\mathrm{p}^2}{R_\mathrm{b}^2} - \frac{1+v}{E^*}\frac{R_\mathrm{p}^2}{R_\mathrm{b}^2}\right]\left(P_0 - \sigma_{r\mathrm{p}}\right)R_0. \tag{23}$$

If the support pressure is greater than or equal to the value of $\sigma_{r\mathrm{p}}$, the division of the surrounding rock in Fig. 3 can be reduced to the bolted region (elastic) and unreinforced region (elastic). Submitting $R_\mathrm{p} = R_0$ and $\sigma_{r\mathrm{p}} = P_i$ into Eq. (16) provides the radial displacement at the tunnel wall in the case without generating the plastic zone.

$$u_{\max} = \left[\frac{1+v}{E^*}\frac{R_\mathrm{b}^2 - R_0^2}{R_\mathrm{b}^2} + \frac{1+v}{E}\frac{R_0^2}{R_\mathrm{b}^2}\right]R_0\left(P_0 - P_i\right). \tag{24}$$

4 Determination of the support pressure

It implies that a considerable displacement of surrounding rock is accepted in the tunnel applying yielding lining. A remarkable increase in the risk of generating loosening rock pressure can be observed in such tunnel, compared with those using the traditional strong supports. The loosening rock pressure is triggered by the excessive rock displacement and directly acts on the lining in the form of gravity. In the tunnel design, it is important to prevent the generation of the loosening rock pressure, so as to avoid the consequent disasters. Caquot considered that the loosening rock pressure was caused by the surrounding rock in the plastic zone and he provided the formula to calculate this pressure as follows [53]:

$$P_\mathrm{a} = k_1\gamma R_0 - k_2 c, \tag{25}$$

where P_a is the loosening rock pressure and γ denotes the rock gravity. For the bolted rock, the cohesion c in Eq. (25) should be replaced with c^*. k_1 and k_2 have the following expressions:

$$k_1 = \frac{1-\sin\varphi}{3\sin\varphi - 1}\left[1 - \left(\frac{R_0}{R_\mathrm{p}}\right)^{\frac{3\sin\varphi-1}{1-\sin\varphi}}\right], \tag{26}$$

$$k_2 = \cot\varphi\left[1 - \left(\frac{R_0}{R_\mathrm{p}}\right)^{\frac{2\sin\varphi}{1-\sin\varphi}}\right], \tag{27}$$

where for the bolted rock, the internal friction angle φ in Eqs. (26) and (27) should be substituted by φ^*.

According to Eq. (25), it can be inferred that there are three cases regarding the calculation of P_a as follows:

$$\begin{cases} P_\mathrm{a} < 0 \\ P_\mathrm{a} = 0 \\ P_\mathrm{a} > 0 \end{cases}. \tag{28}$$

If $P_\mathrm{a} < 0$, it means that the surrounding rock does not generate the loosening rock pressure and the strength of surrounding rock is sufficient to bear its self-gravity. Conversely, it should pay the necessary attention to the loosening rock pressure with $P_\mathrm{a} > 0$. The current support pressure in the condition of $P_\mathrm{a} = 0$ is the critical pressure and it can determine the minimum designed support pressure in this way.

When the rockbolt length L ($R_p - R_0$) is less than the value of $R_p - R_0$, those rockbolts are all placed in the plastic zone and can move with the plastic zone. It increases the possibility of shear slip failure of the surrounding rock. The surrounding rock in the plastic zone can be connected with the stable rock in the elastic zone by using rockbolts and it can play a better role in utilizing the self-bearing capacity of surrounding rock, if the rockbolt length L is higher than this value of $R_p - R_0$. Therefore, it can calculate the minimum designed support pressure by using Eq. (9) from the aspect of rockbolt length ($L = R_p - R_0$). Based on Eqs. (9) and (28), the optimal support pressure $P_{i,\mathrm{opt}}$ (the larger value in the cases considering the loosening rock pressure and rockbolt length) can be determined, and thus, the equilibrium point between the ground and lining can be obtained.

5 Determination of length and yielding stress of highly deformable elements

The aforementioned sections provide the equations for constructing GRC considering rockbolt reinforcement and the optimal support pressure. This section aims to determine the appropriate yielding length and stress of highly deformable elements incorporated in the lining. Figure 4 provides the sketches of the mechanical models of yielding lining before and after deformation. The installation number and length of highly deformable elements in the lining are n and l, respectively.

In the convergence-confinement method, the starting displacement point corresponding to the lining installation is generally determined using the longitudinal displacement profile (LDP) curve. Vlachopoulos and Diederichs [16] used the plastic radius as the fundamental factor and established the mechanical model for calculating LDP curve within elasto-plastic rock.

Define that X represents the distance from the section to the tunnel face. For $X = 0$, i.e., at the tunnel face, it has

$$u_0 = \frac{1}{3} u_{\max} \cdot \exp\left(-0.15 \frac{R_p}{R_0}\right), \tag{29}$$

where u_0 denotes the starting displacement corresponding to the lining installation.

For $X \le 0$, the radial displacement at a specified longitudinal position X can be calculated as

$$u(X) = u_{\max} \cdot u_0^* \cdot \exp\left(\frac{X}{R_0}\right), \tag{30}$$

where u_0^* is equal to $u_0/u_{\max}$.

For $X > 0$, the radial displacement in the section with a distance X can be given by

$$u(X) = u_{\max} \cdot \left[1 - \left(1 - u_0^*\right) \exp\left(-1.5 \frac{X}{R_p}\right)\right]. \tag{31}$$

For a tunnel applying yielding lining, the radial displacement at the tunnel wall consists of three parts after excavation. The first is the initial radial displacement u_0 before installing the lining. The second and third parts are the radial displacements caused by the circumferential shortenings of shotcrete lining and highly deformable elements, respectively.

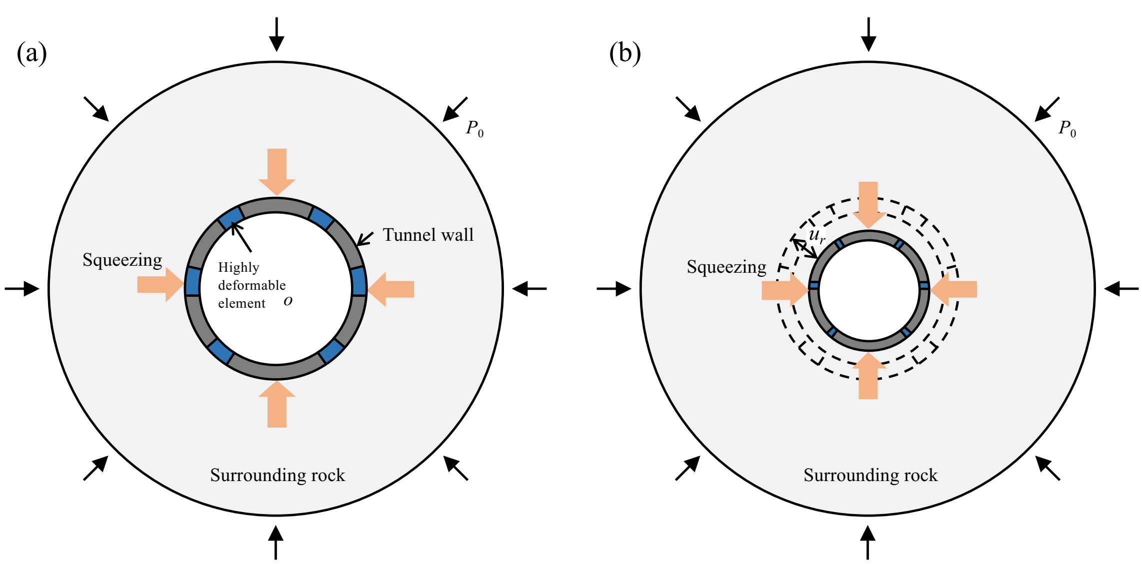

Fig. 4 Mechanical models of yielding lining **a** before and **b** after deformation

Therefore, the total compression length of highly deformable elements in Fig. 4b can be obtained using Eq. (32):

$$\Delta L_{\mathrm{tot}} = 2\pi\left(u_{\max} - u_0 - \beta R_0 \frac{p_{i,\mathrm{opt}}}{K_{\mathrm{s}}}\right), \tag{32}$$

where ΔL_{tot} is the total compression length of highly deformable elements. β denotes the deformation magnification factor considering the shotcrete hardening property, and it usually has the value of 1.1 [56]. K_{s} represents the lining stiffness and can be calculated as [57]

$$K_{\mathrm{s}} = \frac{E_{\mathrm{s}}}{\left(1+\nu_{\mathrm{s}}\right)} \frac{\left[R_0^2 - \left(R_0 - h_{\mathrm{s}}\right)^2\right]}{\left(1-2\nu_{\mathrm{s}}\right)R_0^2 + \left(R_0 - h_{\mathrm{s}}\right)^2}, \tag{33}$$

where E_{s} and ν_{s} are the elastic modulus and Poisson's ratio of shotcrete material, respectively. h_{s} denotes the lining thickness.

For the relationship between the support pressure and tangential stress in the lining, it has

$$\begin{aligned}\sigma_\theta &= \frac{p_i}{h_{\mathrm{s}}}\int_{R_0-h_{\mathrm{s}}}^{R_0}\left\{\left[1+\frac{\left(R_0-h_{\mathrm{s}}\right)^2}{r^2}\right]\Big/\left[1-\frac{\left(R_0-h_{\mathrm{s}}\right)^2}{r^2}\right]\right\}\mathrm{d}r \\ &= \frac{p_i R_0}{h_{\mathrm{s}}}.\end{aligned} \tag{34}$$

According to Eq. (34), the lining thickness can be given by

$$h_{\mathrm{s}} = \delta\frac{p_{i,\mathrm{opt}}R_0}{\sigma_{\mathrm{c}}}, \tag{35}$$

where δ is the safety coefficient of lining. σ_{c} denotes the compressive strength of shotcrete.

If the ΔL_{tot} in Eq. (32) is less than or equal to 0, it implies that the lining is of sufficient bearing capacity to limit rock pressure without being damaged; it is unnecessary to implement highly deformable elements into lining. Conversely, the designed length of highly deformable elements can be obtained using Eq. (36), as the ΔL_{tot} is greater than 0.

$$l = \frac{2\pi\left(u_{\max} - u_0 - \beta R_0\frac{p_{i,\mathrm{opt}}}{K_{\mathrm{s}}}\right)}{n\varepsilon_{\lim}}, \tag{36}$$

where $\varepsilon_{\lim}$ denotes the limit strain of highly deformable elements.

Finally, it can provide the formula for calculating the yielding stress of highly deformable elements using Eq. (34) as follows:

$$\sigma_y = \lambda\frac{p_{i,\mathrm{opt}}R_0}{h_{\mathrm{s}}}, \tag{37}$$

where λ is the reduction factor, usually ranging from 0.4 to 0.6 [58].

Shotcrete exhibits a low strength in the early hardening stage. Remarkably, if this reduction factor is set too high, the shotcrete lining would be damaged or even fail before the yielding of these elements. Instead, the risk that the surrounding rock falls off suddenly can be highly increased during the yielding of highly deformable elements, as this reduction factor has a small value. The extreme case is that the rock displaces freely without installing any supports; absolutely, it is not allowed in the large deformation tunnels in severe squeezing ground.

For the convenience of applying the proposed design model, Fig. 5 exhibits the flow chart. Overall, the calculation process can be divided into four steps as follows:

Step 1: Input the parameters of rockbolt and rock and submitting them into Eqs. (1), (4), (6), and (7) provides the

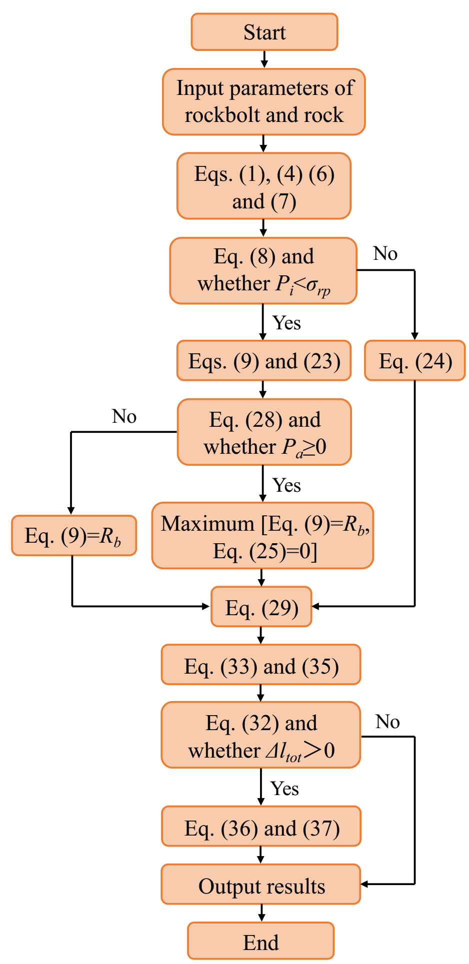

Fig. 5 Flow chart of calculation process

elastic modulus E^*, cohesion c^*, and internal friction angle φ^* of bolted rock.

Step 2: Using Eq. (8) provides σ_{rp}. If P_i is smaller than σ_{rp}, submitting P_i into Eq. (9) provides the plastic radius R_p, and then the plastic ground reaction curve can be obtained using Eq. (23). It can provides the elastic ground reaction curve using Eq. (24), as P_i is larger than σ_{rp}.

Step 3: Under the condition that P_i is smaller than σ_{rp}, judge whether the loosening rock pressure P_a is larger than or equal to 0 using Eq. (28). If yes, define that R_p is equal to R_b using Eq. (9) and P_a is equal to zero. It provides two values of support pressure P_i and it requires the larger one as the optimal support pressure. If P_i is larger than σ_{rp}, we can use this value as the support pressure.

Step 4: Using Eq. (29) provides the starting displacement corresponding to the lining installation. Furthermore, using Eqs. (33) and (35) provides the lining thickness h_s and stiffness K_s. Judge whether ΔL_{tot} is greater than 0 using Eq. (32). If yes, using Eqs. (36) and (37) provides the length and yielding stress of highly deformable elements. If no, it means that the current strong supports are heavy enough to limit rock pressure and the installation of highly deformable elements is unnecessary in the lining.

Table 1 Parameters in the Xinhua tunnel obtained from field data

Item	Value
Initial ground stress, P_0 (MPa)	15
Tunnel radius, R_0 (m)	6.2
Elastic modulus of rock, E (MPa)	520
Poisson's ratio of rock, ν	0.36
Cohesion of rock, c (MPa)	0.85
Internal friction of rock, φ (°)	28
Dilatancy coefficient of rock	1.3
S_r (m)	1
S_l (m)	1
Elastic modulus of shotcrete, E_s (MPa)	25,000
Poisson's ratio of shotcrete, ν_s	0.2
Thickness of shotcrete lining, h_s (mm)	240

$$u_{\max} = \frac{1+\nu}{E} R_0 \left(P_0 - P_i\right), \quad (38)$$

$$u_{\max} = \frac{R_0\left(P_0 - \sigma_{rp}\right)}{2G} \left\{ 1 + \left[\left(\frac{R_p}{R_0} \right)^2 - 1 \right] \right\}. \quad (39)$$

6 Engineering application

6.1 Reduction to the proposed solutions

The previous researches have provided the GRC without considering rockbolt reinforcement or plastic dilatancy [53]. Equations (38) and (39) show the formulas for calculating the elastic and plastic GRC without considering these factors, respectively. It can be found that if submitting $E^*=E$, $R_b=R_p$ and $\alpha=1$ into Eq. (23) (namely, the rockbolt reinforcement and plastic dilatancy are not taken into account), it can be reduced into Eq. (39). If submitting $E^*=E$ and $R_b=R_0$ into Eq. (24), it can be reduced into Eq. (38). In other words, the proposed equations for calculating CRC in this study can be reduced to those without considering rockbolt reinforcement and plastic dilatancy.

6.2 Application in the Xinhua tunnel

The Xinhua tunnel was a critical part for the Dalin railway from Dali to Lincang, Yunnan province, China. It had a total length of 12.332 km and the maximum buried depth was approximately equal to 1070 m. As shown in Fig. 6a, it provides the detailed longitudinal profile of the Xinhua tunnel. This tunnel was excavated in the severe squeezing ground and the quality of rock was very poor. In the original scheme the supports consisting of 6 m long rockbolts and 24 cm thick shotcrete lining were used. Unfortunately, they could not limit rock displacement well and the severe support failure was observed in the Xinhua tunnel, as shown in Fig. 6b. The parameters of surrounding rock and supports in the Xinhua tunnel were obtained from the field data and are listed in Table 1.

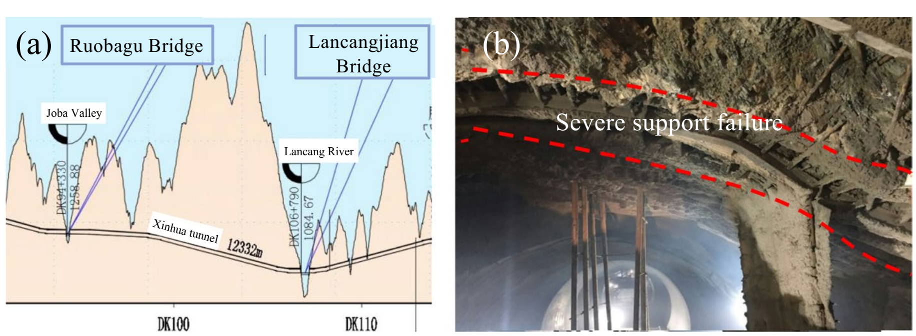

Fig. 6 Geographical information of the Xinhua tunnel **a** longitudinal profile; **b** severe support failure

As shown in Fig. 7, the convergence-confinement curves in the Xinhua tunnel applying the strong supports are plotted. The results reveal that the strong supports completed a small elastic displacement followed by a large plastic displacement. The maximum displacement of surrounding rock reaches 382.6 mm and the supports generate the displacement of 287.4 mm at the equilibrium point between GRC and SCC (support characteristic curve). The tunnel displacement calculated by using the analytical solution has a good agreement with the monitoring arch settlement in the Xinhua tunnel, which value was approximately equal to 306.9 mm (not monitored thereafter). According to the theoretical results, the strong supports exhibit a plastic displacement of 281.8 mm in the Xinhua tunnel and such a large plastic displacement cannot be tolerated by the strong supports. The severe support failure in the Xinhua tunnel can thus be well explained by these analytical results.

The ultimate bearing capacity of the strong supports ($\sigma_c = 25$ MPa and $h_s = 24$ cm) in the Xinhua tunnel was equal to 0.968 MPa, which is calculated by using Eq. (34). It is far from the required support pressure that is sufficient to strictly limit rock displacement. If the strong supports are applied without being damaged in the Xinhua tunnel, it needs to provide a support pressure of approximately 5 MPa from the convergence-confinement curves in Fig. 8. This requires that the lining should have a thickness of 124 cm, which seems to be an impractical idea in the actual tunnel engineering.

If the yielding lining is employed in the Xinhua tunnel, its design parameters can be obtained by following the flow chart in Fig. 5. In this calculation, the plastic radius of surrounding rock is regarded to be equal to 12.2 m (R_b), with the intention to maximize the utilization of rockbolt capacity. The required support pressure provided by yielding lining should reach 0.866 MPa using Eq. (9) and the required lining thickness should have 28 cm using Eq. (35), when the lining safety coefficient is selected as 1.3. Furthermore, by using Eqs. (23) and (29), it determines the maximum tunnel displacement ($u_{max} = 400.3$ mm) and the starting displacement ($u_0 = 99.2$ mm) under the condition of support pressure of 0.866 MPa. The convergence-confinement curves in the Xinhua tunnel applying yielding lining are shown in Fig. 8.

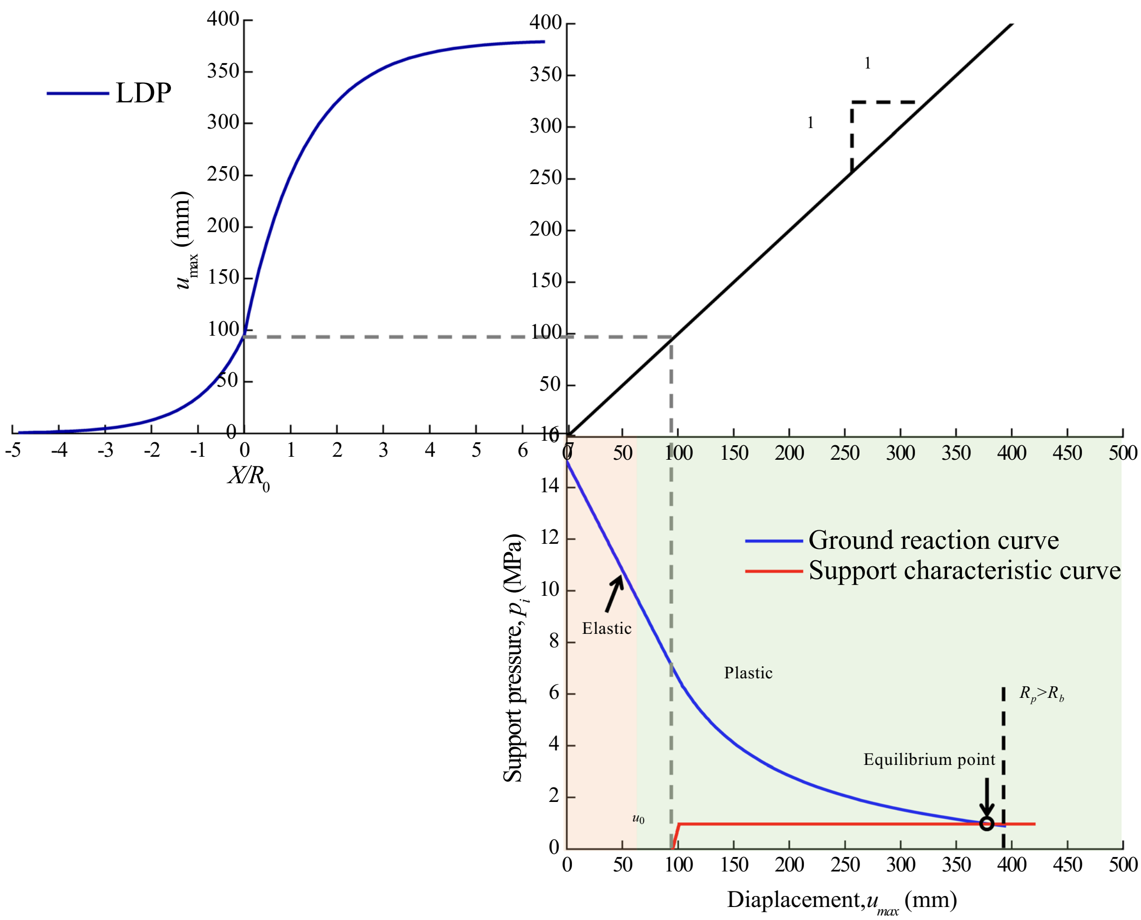

Fig. 7 Convergence-confinement curves in the Xinhua tunnel employing strong supports

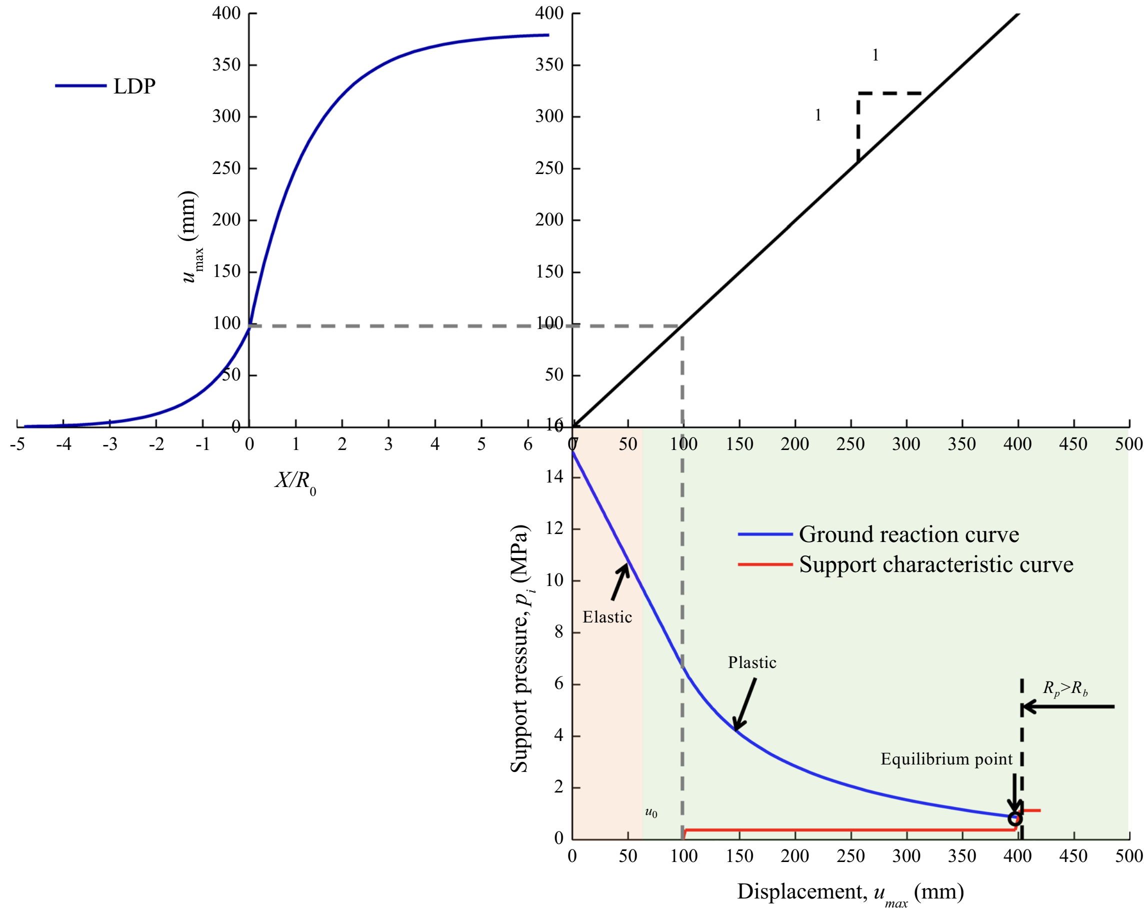

Fig. 8 Convergence-confinement curves in the Xinhua tunnel employing yielding lining

Then, the designed total length (nl) of highly deformable elements incorporated in the lining should has 371.7 cm using Eq. (36), provided that the ultimate strain of highly deformable elements is equal to 50% and $\beta = 1.1$. Referencing the final installation number of highly deformable elements in the lining in the Saint Martin La Porte access tunnel [48], the element installation number in the Xinhua tunnel is determined to be equal to 9. Therefore, the designed length of each element has 41.3 cm. When the reduction factor λ is 40%, the yielding stress of highly deformable elements σ_y is required to be equal to 7.673 MPa using Eq. (37). In addition, it should highlight that it does not generate loosening rock pressure using such support parameters.

Furthermore, it can be found from the support characteristic curve in Fig. 8 that the yielding lining firstly shows an elastic displacement before the highly deformable elements yield. This process has a relatively short displacement span. The following stage is regarded as the stage of rock displacement release through the plastic shortenings of highly deformable elements. The rock displacement allowed is approximately 298.9 mm in this stage. The support characteristic curve quickly has an intersection with the ground reaction curve after the ultimate strains of highly deformable elements are obtained. At this time, the lining is still in the elastic state. In addition, it still has the capacity to tolerate an additional rock pressure, because the lining safety coefficient is considered in the design model. By comparing the results in Figs. 7 and 8, the maximum rock displacements are almost equal under the condition of strong and yielding linings. The strong supports generate severe failure represented by the large plastic displacement, but the yielding lining remains in safety. This indicates the feasibility of applying yielding lining in the Xinhua tunnel.

7 Parametric investigation

According to the proposed design model, the influences of rock cohesion and internal friction angle, rockbolt length, and initial ground stress are discussed in this section. We still assume that it maximizes the utilization of bearing capacity of rockbolts and does not generate loosening rock pressure in the tunnel. Except those parameters discussed in each section, the involved parameters in the calculation are obtained from the Xinhua tunnel (Table 1).

7.1 Cohesion and internal friction angle of rock

The rock cohesion and internal friction angle determine the support design majorly. The influence of rock cohesion is studied firstly. As shown in Fig. 9, the curves for the support pressure, lining thickness, tunnel displacement, and element length with the change of rock cohesion are plotted, respectively. These curves are drawn for rock cohesion $c=0.1$, 0.2, 0.3, 0.4, and 0.5 MPa.

It can be seen from Fig. 9 that the required support pressure remarkably varies with rock cohesion; correspondingly, the lining thickness shows a great change as well. The required support pressure and lining thickness are 1.302 MPa and 42 cm, respectively, with the rock cohesion of 0.1 MPa. The support pressure and lining thickness decrease to 0.595 MPa and 20 cm, respectively, when the rock cohesion increases to 0.5 MPa. The change of lining thickness is linearly related to support pressure. By comparing the tunnel displacements in these five cases, it is interesting to find that the maximum tunnel displacement occurs accompanied by the maximum rock cohesion; the maximum tunnel displacement is equal to 477.5 mm. This is because a higher rock cohesion leads to a smaller support pressure at the premises of maximizing the utilization of rockbolt capacity and not generating loosening rock pressure. A smaller support pressure further causes a larger tunnel displacement. In spite of this, the tunnel displacement increases by only 23.3 mm with rock cohesion ranging from 0.1 to 0.5 MPa, which is not a high increment compared with the total tunnel displacement. The lengths of highly deformable elements calculated in the five cases are 48.4, 49.1, 49.7, 50.2, and 50.9 mm, respectively. It can be found that their value difference can be ignored due to the small change of tunnel displacement. The yielding stress of highly deformable element is determined to be equal to 9.621 MPa, which is only associated with shotcrete strength. In general, the required support pressure and lining thickness both decrease significantly with rock cohesion. By comparison, the influence of cohesion on the parameters of highly deformable elements can almost be neglected, although it increases by 500%.

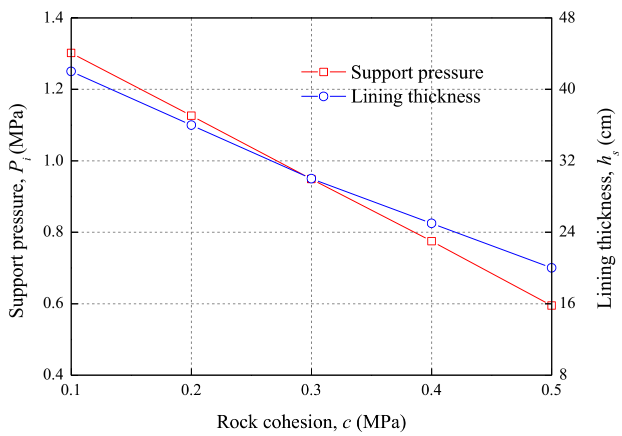

(a)

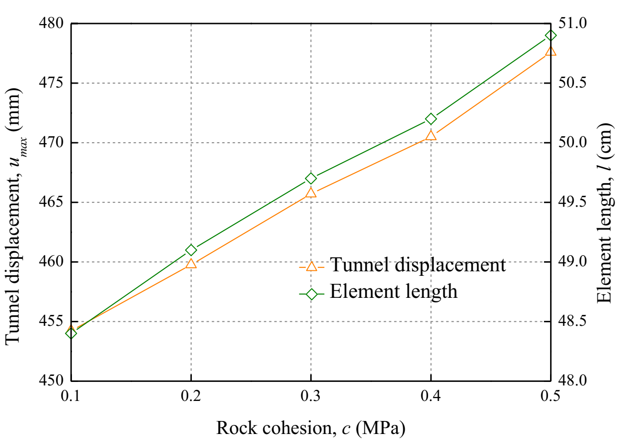

(b)

Fig. 9 Influences of rock cohesion on **a** support pressure and lining thickness; **b** tunnel displacement and element length

Figure 10a illustrates the influences of rock internal friction angle on the support pressure and lining thickness; Fig. 10b shows its influences on the tunnel displacement and element length. The rock internal friction angles of 22°, 23°, 24°, 25°, and 26° are chosen in the calculation. The same change trends of the support pressure, lining thickness, tunnel displacement, and element length can be observed, compared with those as rock cohesion increases. The required support pressure and lining thickness decrease, when the internal friction angle increases; conversely, the tunnel displacement and length of highly deformable element show an increasing trend. However, by comparison, the rock internal friction angle seems to have a higher impact than the rock cohesion, being reflected by the increment or decrement values of these parameters. The support pressure and lining thickness decrease by 0.905 MPa and 29 cm, respectively, as the rock internal friction angle increases from 22° to 26°. The tunnel displacement increase from 414.8 to 477.5 mm and the element length increases from 49.7 to 57.3 cm.

7.2 Rockbolt length

The rock mechanical performance is significantly improved after using rockbolt reinforcement. In the proposed model, the influences caused by the changes of rockbolt radius and installation parameters (s_r, s_l) can be considered through changing rock cohesion and internal friction angle. The influences of rock cohesion and internal friction angle have

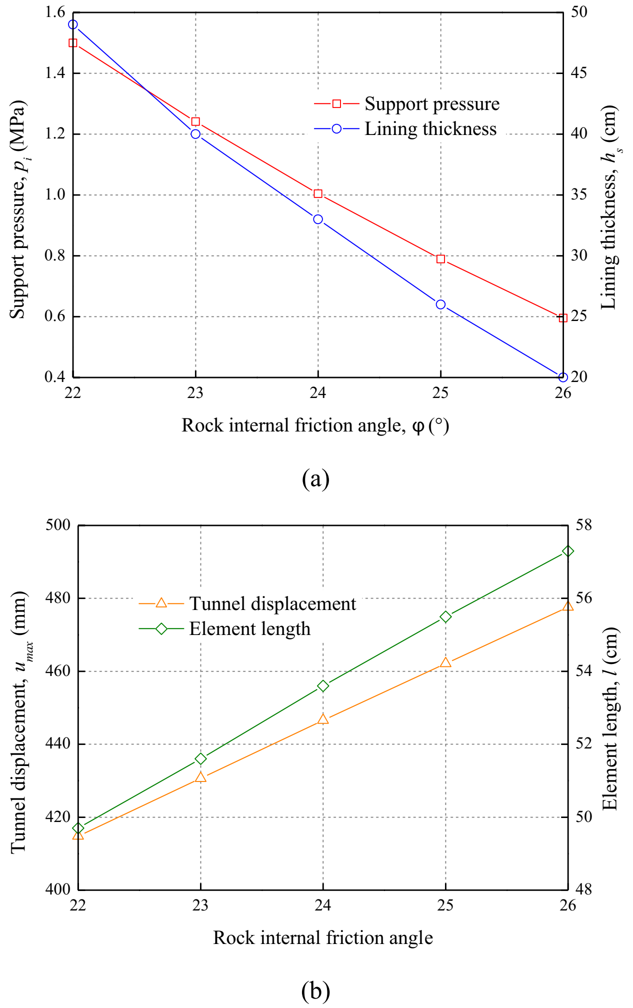

Fig. 10 Influences of rock internal friction angle on **a** support pressure and lining thickness; **b** tunnel displacement and element length

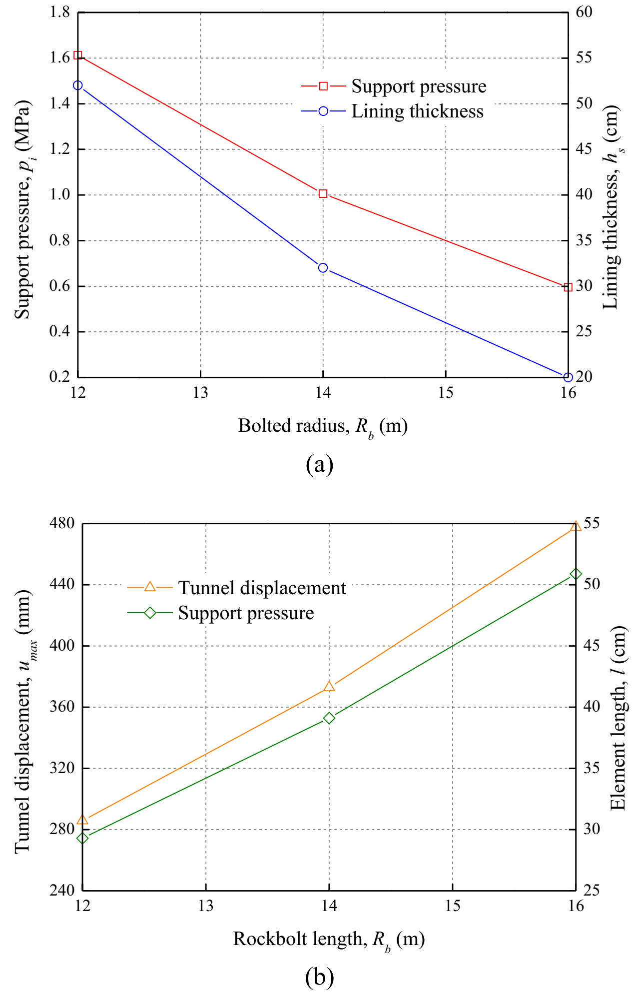

Fig. 11 Influences of rockbolt length on **a** support pressure and lining thickness; **b** tunnel displacement and element length

been discussed in Sect. 7.1. This section aims to analyze the influences of reinforcement area characterized by rockbolt length ($R_b - R_0$). As shown in Fig. 11, these curves are plotted with the bolted rock radius ($R_0 + l_b$) of 12, 14, and 16 m, respectively.

As shown in Fig. 11, the rockbolt length has significant influences on the support pressure, lining thickness, tunnel displacement, and element length. The required support pressure and lining thickness decrease sharply as the rockbolt length increases. The support pressures are 1.612, 1.005, and 0.595 MPa, respectively, and the lining thicknesses are 52, 32, and 20 cm, respectively, corresponding to the bolted rock radius of 12, 14, and 16 m, respectively. The increase in rockbolt length implies an increase in the bolted rock area that has a stronger anti-deforming capacity. However, an abnormal phenomenon that the tunnel displacement shows a remarkable increase with the rockbolt length can be observed from Fig. 11; the tunnel displacement increases from 285.7 to 477.6 mm as the rockbolt length increases from 12 to 16 m. This is because the required support pressure (lining thickness) decreases with the rockbolt length under the condition of maximizing the rockbolt capacity. The decrease in support pressure can lead to an increase in tunnel displacement inevitably. Although the increase in rockbolt length should cause a decrease in tunnel displacement, compared with the influence of increasing rockbolt length on tunnel displacement, it has a greater impact by decreasing in support pressure. Therefore, the tunnel displacement exhibits an increasing trend, which is together caused by an increase in rockbolt length and the decrease in support pressure. In these three cases, the designed lengths of highly deformable elements are equal to 29.3, 39.1, and 50.9 cm, respectively. Based on the results, it can be concluded that the rockbolt reinforcement can play a significant role in improving rock stability and the application of yielding lining can make full use of rock self-bearing capacity.

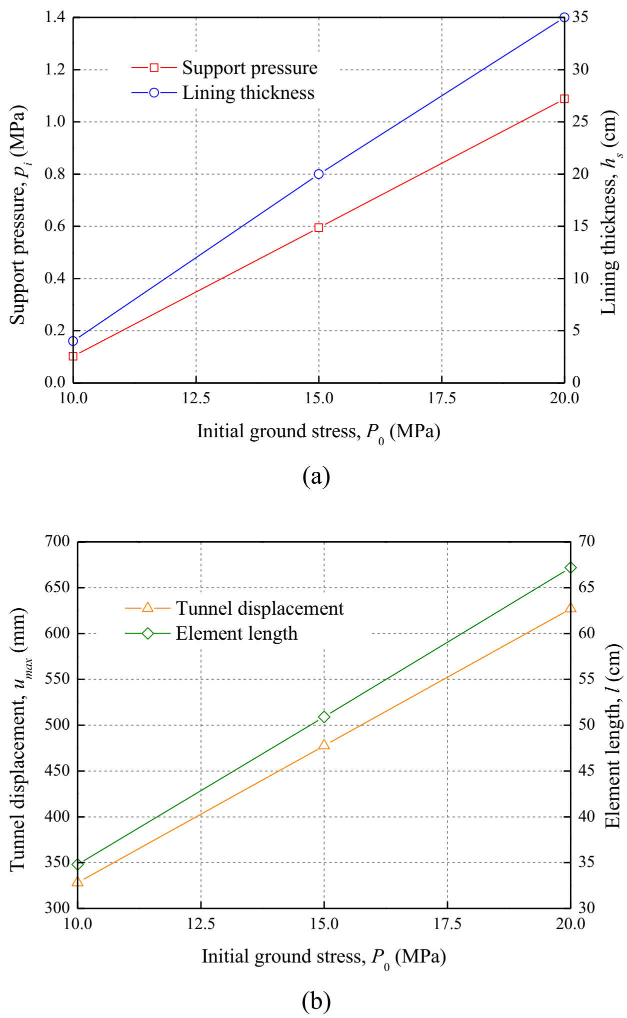

Fig. 12 Influences of initial ground stress on **a** support pressure and lining thickness; **b** tunnel displacement and element length

7.3 Initial ground stress

The initial ground stress level affects the support type selection and design parameters directly. The initial ground stresses of 10, 15, and 20 MPa are applied in the calculation. The analysis results are presented in Fig. 12.

As shown in Fig. 12, the required support pressure and lining thickness are only equal to 0.102 MPa and 4 cm, respectively, when the initial ground stress is 10 MPa. Simultaneously, the tunnel displacement has 328.2 mm and the length of highly deformable elements is equal to 34.8 cm. It almost means that the lining is not required any more in this case. Furthermore, the increment of 0.986 MPa in support pressure and the increment of 31 cm in lining thickness can be observed as the initial ground stress increases from 10 to 20 MPa. Correspondingly, the tunnel displacement increases to 627 mm and the length of highly deformable elements increases to 67.2 cm. The results imply that it may be feasible to apply strong supports to stabilize the surrounding rock at low ground stress level. If the tunnel is subjected to high ground stress (related to rock quality), it is necessary to apply yielding lining to avoid support failure.

8 Conclusions

The design of rockbolt-reinforced tunnel using yield lining is studied from the perspective of the convergence-confinement method. The equations to determine the mechanical parameters (elastic modulus, rock cohesion, and internal friction angle) of bolted rock are provided and the mechanical model of a circular bolted tunnel is established. The equations for constructing the ground reaction curve are provided, which take the rockbolt reinforcement and rock shear dilatancy into account. The required minimum support pressure is determined following the assumptions of maximizing the utilization of rockbolt bearing capacity and generating no loosening rock pressure. The equations to determine the lining thickness and the length and yielding stress of highly deformable elements are provided, where the lining safety coefficient and shotcrete hardening property are considered.

The proposed equations for GRC in this study can be reduced to those that do not consider rockbolt reinforcement and rock shear dilatancy. A good application of the design method of yielding lining is well realized in the Xinhua tunnel. The parametric analysis indicates that the required support pressure and lining thickness decrease significantly as the rock cohesion or internal friction angle increases; the increases in tunnel displacement and length of highly deformable elements can be observed. By comparison, the rock internal friction angle exhibits a higher impact on tunnel displacement and element length. The increase in rockbolt length causes the decrease in the required support pressure and lining thickness. But the tunnel displacement and length of highly deformable elements increase unexpectedly. This is together caused by an increase in rockbolt length and the decrease in support pressure and the influence of the latter is higher than that of the former. When the initial ground stress is high (related to rock quality), it is necessary to make full use of rock self-bearing capacity and the application of yielding lining is a good choice.

Acknowledgements The authors thank for the financial supports of the National Natural Science Foundation of China (No. 12202334).

Data availability Data will be made available on request.

Declarations

Conflict of interest The authors confirm that they have no conflicts of interest for this work.

Ethical statement The authors state that this work was conducted according to ethical standards.

References

1. Barla G. Full-face excavation of large tunnels in difficult conditions. J Rock Mech Geotech Eng. 2016;8(3):294–303.
2. Hoek E, Guevara R. Overcoming squeezing in the Yacambú-Quibor tunnel, Venezuela. Rock Mech Rock Eng. 2009;42:389–418.
3. Kovári K. Design methods with yielding support in squeezing and swelling rocks. In: Proceedings of the world tunnel congress, Budapest, Hungary, 2009.
4. Moritz B. Yielding elements-requirements, overview and comparison. Geomech Tunn. 2011;4(3):221–36.
5. Wu K, Shao ZS, Sharifzadeh M, Hong SY, Qin S. Analytical computation of support characteristic curve for circumferential yielding lining in tunnel design. J Rock Mech Geotech Eng. 2022;14(1):144–52.
6. Ci X, Liu XY, Tan XJ, Yang DS, Tian HM, Chen WZ. Numerical simulation on progressive failure of yielding support material for squeezing tunnel. Arch Civ Mech Eng. 2023;24:9.
7. Cantieni L, Anagnostou G. The interaction between yielding supports and squeezing ground. Tunn Undergr Space Technol. 2009;24(3):309–22.
8. Qin S, Shao ZS, Yuan B, Zheng XM, Zhao NN, Wu K. A simple prediction model for mechanical response of lined tunnels incorporating yielding elements. Int J Appl Mech. 2023;15(5):2350031.
9. Xu JF, Xie XY, Tang GJ, Zhou B, Xu DL, Huang Y. A new adaptive compressible element for tunnel lining support in squeezing rock masses. Tunn Undergr Space Technol. 2023;137: 105124.
10. Yan Q, Li SC, Xie C, Li Y. Analytical solution for bolted tunnels in expansive loess using the convergence-confinement method. Int J Geomech. 2018;18(1):04017124.
11. Zhao JS, Duan SQ, Chen BR, Li L, He BG, Li PX, Liu GF. Failure mechanism of rock masses with complex geological conditions in a large underground cavern: a case study. Soil Dyn Earthq Eng. 2024;177: 108439.
12. Chen YL, Teng JY, Bin Sadiq RA, Zhang K. Experimental study of bolt-anchoring mechanism for bedded rock mass. Int J Geomech. 2020;20(4):04020019.
13. Chen Y, Li CC. Influences of Loading condition and rock strength to the performance of rock bolts. Geotech Test J. 2015;38(2):208–18.
14. Cai Y, Esaki T, Jiang YJ. An analytical model to predict axial load in grouted rock bolt for soft rock tunnelling. Tunn Undergr Space Technol. 2004;19(6):607–18.
15. Li C. A practical problem with threaded rebar bolts in reinforcing largely deformed rock masses. Rock Mech Rock Eng. 2007;40:519–24.
16. Vlachopoulos N, Diederichs MS. Improved longitudinal displacement profiles for convergence confinement analysis of deep tunnels. Rock Mech Rock Eng. 2009;42:131–46.
17. Paraskevopoulou C, Diederichs M. Analysis of time-dependent deformation in tunnels using the convergence-confinement method. Tunn Undergr Space Technol. 2018;71:62–80.
18. De La Fuente M, Taherzadeh R, Sulem J, Nguyen XS, Subrin D. Applicability of the convergence-confinement method to full-face excavation of circular tunnels with stiff support system. Rock Mech Rock Eng. 2019;52:2361–76.
19. Alejano LR, Alonso E, Rodriguez-Dono A, Fernandez-Manin G. Application of the convergence-confinement method to tunnels in rock masses exhibiting Hoek-Brown strain-softening behaviour. Int J Rock Mech Min Sci. 2010;47(1):150–60.
20. Gschwandtner GG, Galler R. Input to the application of the convergence confinement method with time-dependent material behaviour of the support. Tunn Undergr Space Technol. 2012;27(1):13–22.
21. Ravandi EG, Rahmannejad R. Wall displacement prediction of circular, D shaped and modified horseshoe tunnels in non-hydrostatic stress fields. Tunn Undergr Space Technol. 2013;34:54–60.
22. Wang ZC, Shi YF, Xie YL, Zhang MZ, Liu T, Li C, Zhang CP. Support characteristic of a novel type of support in loess tunnels using the convergence-confinement method. Int J Geomech. 2021;21(10):06021026.
23. Oke J, Vlachopoulos N, Diederichs M. Improvement to the convergence-confinement method: inclusion of support installation proximity and stiffness. Rock Mech Rock Eng. 2018;51:1495–519.
24. Wu K, Song JA, Zhao NN, Shao ZS. Study on the time-dependent interaction between surrounding rock and yielding supports in deep soft rock tunnels. Int J Numer Anal Met Geomech. 2024;48:566–87.
25. Lackner R, Macht J, Hellmich C, Mang HA. Hybrid method for analysis of segmented shotcrete tunnel linings. J Geotech Geoenviron Eng. 2002;128(4):298–308.
26. Schubert W, Brunnegger S. Further development of yielding elements and connecting elements for shotcrete. Geomech Tunn. 2018;11(5):575–81.
27. Zhang CX, Tan XJ, Tian HM, Chen WZ. Lateral compression and energy absorption of foamed concrete-filled polyethylene circular pipe as yielding layer for high geo-stress soft rock tunnels. Int J Min Sci Technol. 2022;32(5):1087–96.
28. Verient M, Schubert W, Radoncic N, Kluckner A. Investigations on telescope yielding elements with porous filling. In: ISRM regional symposium EUROCK 2015 & 64th geomechanics colloquium-future development of rock mechanics, Salzburg, Austria, 2015.
29. Wu K, Shao ZS, Qin S, Wei W, Chu ZF. A critical review on the performance of yielding supports in squeezing tunnels. Tunn Undergr Space Technol. 2021;115: 103815.
30. Barla G, Debernardi D, Sterpi D. Time-dependent modeling of tunnels in squeezing conditions. Int J Geomech. 2012;12(6):697–710.
31. Qiu W, Wang G, Gong L, Shen Z, Li C, Dang J. Research and application of resistance-limiting and energy-dissipating support in large deformation tunnel. Chin J Rock Mech Eng. 2018;37(8):1785–95.
32. Zheng Q, Zhang X, Shen YS, Qiu JT, Wang YD, Chen KF. Failure mechanism of segmental lining structure in fault-crossing tunnel: an experimental and numerical investigation. J Cent South Univ. 2023;30(7):2392–410.
33. Yang YZ, Wang YJ, Wu K. Numerical study on dynamic fracture and energy transformation characteristics of rock unloading failure under identical energy stored levels. Int J Geomech. 2023;23(12):04023217.
34. Liu Y, Sulem J, Subrin D, Tran-Manh H, Humbert E. Time-dependent behavior of Saint-Martin-La-Porte exploratory galleries: field data processing and numerical modeling of excavation in squeezing rock conditions. Int J Geomech. 2021;21(12):04021239.
35. Ramoni M, Anagnostou G. The interaction between shield, ground and tunnel support in TBM tunnelling through squeezing ground. Rock Mech Rock Eng. 2011;44:37–61.
36. Tian HM, Chen WZ, Tan XJ, Yang DS, Wu GJ, Yu JX. Numerical investigation of the influence of the yield stress of the yielding element on the behaviour of the shotcrete liner for yielding support. Tunn Undergr Space Technol. 2018;73:179–86.
37. Yang K, Yan Q, Shi Z, Zhang C, Ma S. Numerical study on the mechanical behavior of shotcrete lining with yielding

support in large deformation tunnel. Rock Mech Rock Eng. 2023;56:1563–84.
38. Hammer AL, Hasanpour R, Hofmann C, Thewes M. Numerical analysis of interaction behavior of yielding supports in squeezing ground. In: Numerical methods in geotechnical engineering IX. Boca Raton: CRC Press; 2018.
39. Cai WQ, Zhu HH, Liang WH, Wang XJ, Wei XY, Su CL. Post-peak dilatancy model for soft rock and its application in a deep tunnel excavated in strain-softening rock mass. J Rock Mech Geotech Eng. 2023;15(3):683–701.
40. Wu K, Shao ZS, Qin S. An analytical design method for ductile support structures in squeezing tunnels. Arch Civ Mech Eng. 2020;20(3):91.
41. Wu K, Shao ZS, Jiang YL, Zhao NN, Qin S, Chu ZF. Determination of stiffness of circumferential yielding lining considering the shotcrete hardening property. Rock Mech Rock Eng. 2023;56:3023–36.
42. Lei SX, Zhao W. Study on mechanism of circumferential yielding support for soft rock tunnel with large deformation. Rock Soil Mech. 2020;41(3):1039–47.
43. Mezger F, Ramoni M, Anagnostou G. Options for deformable segmental lining systems for tunnelling in squeezing rock. Tunn Undergr Space Technol. 2018;76:64–75.
44. Tian HM, Tian Y, Chen WZ, Tan XJ, Shu XY, Liu XL. Design of the yielding support used highly deformable elements for a tunnel excavated in squeezing rock. J Mt Sci. 2023;20(5):1458–68.
45. Radoncic N, Schubert W, Moritz B. Ductile support design. Geomech Tunn. 2009;2(5):561–77.
46. Sakai K, Schubert W. Study on ductile support system by means of convergence confinement method. In: 5th ISRM Young scholars' symposium on rock mechanics and international symposium on rock engineering for innovative future, 2019.
47. Kolymbas D. Stress and deformation fields around a deep circular tunnel. In: Tunnelling and tunnel mechanics: a rational approach to tunneling. Berlin/Heidelberg: Springer; 2005.
48. Weidinger F, Lauffer H. The Tauern tunnel first and second tubes from the contractor's viewpoint. Geomech Tunn. 2009;2:24–32.
49. Bonini M, Barla G. The Saint Martin La Porte access adit (Lyon-Turin Base Tunnel) revisited. Tunn Undergr Space Technol. 2012;30:38–54.
50. Dalgıç S. Tunneling in squeezing rock, the Bolu tunnel, Anatolian Motorway, Turkey. Eng Geol. 2002;67(1–2):73–96.
51. Zhao NN, Shao ZS, Wu K. Analytical approach to predicting the time-dependent response of deep soft rock tunnels considering the compressible layer and stress path effects. Int J Geomech. 2023;23(6):04023070.
52. Indraratna B, Kaiser PK. Analytical model for the design of grouted rock bolt. Int J Numer Anal Met Geomech. 1990;14(4):227–51.
53. Zheng YR, Zhu HH, Fang ZC, Liu HR. The stability analysis and design theory of surrounding rock of underground engineering. Beijing: China Communications Press; 2012.
54. Xu C, Xia CC, Han CL. Elastoplastic solutions for deep tunnel excavation in weak rocks with high geostress considering different stress release measures. Int J Appl Mech. 2022;14(8):2250077.
55. Du JM, Fang Q, Wang G, Wang J. Analytical solution of a circular lined tunnel with alterable mechanical property under hydrostatic stress and internal pressure. J Cent South Univ. 2022;29(8):2757–70.
56. Wu K, Shao ZS, Sharifzadeh M, Chu ZF, Qin S. Analytical approach to estimating the influence of shotcrete hardening property on tunnel response. J Eng Mech. 2022;148(1):04021127.
57. Chu ZF, Wu ZJ, Liu QS, Weng L, Xu XY. Viscos-elastic-plastic solution for deep buried tunnels considering tunnel face effect and sequential installation of double linings. Comput Geotech. 2024;165: 105930.
58. Tian HM, Chen WZ, Yang DS, Wu GJ, Tan XJ. Numerical analysis on the interaction of shotcrete liner with rock for yielding supports. Tunn Undergr Space Technol. 2016;54:20–8.